Remark 9: For the example given by (51), there exist positive definite symmetric matrices $\boldsymbol{P}, \boldsymbol{W}_{01}, \boldsymbol{W}_{10}$ and a positive definite diagonal matrix $\boldsymbol{C}(=\boldsymbol{D})$ for which (4) is satisfied, while there do not exist positive definite symmetric matrices $\boldsymbol{H}, \boldsymbol{W}_{01}, \boldsymbol{W}_{10}$ for which (7a) and (7b), with $L = 1$, is satisfied. Thus, pertaining to saturation nonlinearities, (4) may lead to results not covered by (7a) and (7b).

Remark 10: For all of the examples presented above [see (37), (49), (51)–(53)], Theorem 3 fails as global asymptotic stability test; to the contrary, Corollary 1 or Corollary 2, as the case may be, establishes global asymptotic stability for these examples. Thus, even Corollary 1 and Corollary 2 (which are special cases of Theorems 4 and 5, respectively) may provide results not covered by Theorem 3.

IV. Extensions to Quantization Nonlinearities

Recall that the quantization nonlinearities are confined to the sector $[0, \alpha]$, i.e.,

$$f_i(0) = 0, \qquad 0 \le f_i(y_i(k, l))y_i(k, l) \le \alpha y_i^2(k, l) \quad i = 1, 2, \ldots, n \tag{54a}$$

$$\alpha = 1(\alpha = 2) \text{ for magnitude truncation (roundoff) nonlinearities.} \tag{54b}$$

As an extension of a well-known 1-D approach [14], the following is easily arrived at.

Theorem 7: The nonlinear LSS model given by (1a)–(1e) and (54) is globally asymptotically stable provided there exist an $n \times n$ positive definite diagonal matrix $\boldsymbol{D}$ and $n \times n$ positive definite symmetric matrices $\boldsymbol{P}, \boldsymbol{W}_{01}, \boldsymbol{W}_{10}$ satisfying (10e) and

$$\left[\begin{array}{cc|c} \boldsymbol{P}^{T/2}\boldsymbol{W}_{01}\boldsymbol{P}^{1/2} & \boldsymbol{0} & -\alpha\boldsymbol{A}^T\boldsymbol{D} \\ \boldsymbol{0} & \boldsymbol{P}^{T/2}\boldsymbol{W}_{10}\boldsymbol{P}^{1/2} & \\ \hline -\alpha\boldsymbol{D}\boldsymbol{A} & & 2\boldsymbol{D} - \boldsymbol{P} \end{array}\right] > \boldsymbol{0}. \tag{55}$$

V. Conclusion

This paper establishes new criteria for the global asymptotic stability of 2-D digital filters described by the Fornasini–Marchesini second LSS model with overflow nonlinearities. The criteria, for saturation and triangular arithmetics, imply overflow stability for a broader class of *A*, as compared to [9]; for other overflow nonlinearities, the present approach and [9] are supplement to each other. The approach leads to a more relaxed saturation overflow stability condition, as compared to [11]. A limit cycle-free realizability condition pertaining to quantization nonlinearities is presented.

References

[1] D. Liu and A. N. Michel, "Stability analysis of state-space realizations for two-dimensional filters with overflow nonlinearities," *IEEE Trans. Circuits Syst. I*, vol. 41, pp. 127–137, Feb. 1994.

[2] S. G. Tzafestas, A. Kanellakis, and N. J. Theodorou, "Two-dimensional digital filters without overflow oscillations and instability due to finite word length," *IEEE Trans. Signal Processing*, vol. 40, pp. 2311–2317, Sept. 1992.

[3] C. Xiao and D. J. Hill, "Stability and absence of overflow oscillations for 2-D discrete-time systems," *IEEE Trans. Signal Processing*, vol. 44, pp. 2108–2110, Aug. 1996.

[4] H. Kar and V. Singh, "Stability analysis of 2-D state-space digital filters using Lyapunov function: A caution," *IEEE Trans. Signal Processing*, vol. 45, pp. 2620–2621, Oct. 1997.

[5] P. H. Bauer and K. R. Ralev, "Comments on Stability and absence of overflow oscillations for 2-D discrete-time systems," *IEEE Trans. Signal Processing*, vol. 46, pp. 803–804, Mar. 1998.

[6] C. Xiao and D. J. Hill, "Reply to 'Comments on Stability and absence of overflow oscillations for 2-D discrete-time systems'," *IEEE Trans. Signal Processing*, vol. 47, p. 2599, Sept. 1999.

[7] L.-J. Leclerc and P. H. Bauer, "New criteria for asymptotic stability of one- and multidimensional state-space digital filters in fixed-point arithmetic," *IEEE Trans. Signal Processing*, vol. 42, pp. 46–53, Jan. 1994.

[8] C. Xiao, D. J. Hill, and P. Agathoklis, "Stability and the Lyapunov equation for n-dimensional digital systems," *IEEE Trans. Circuits Syst. I*, vol. 44, pp. 614–621, July 1997.

[9] D. Liu, "Lyapunov stability of two-dimensional digital filters with overflow nonlinearities," *IEEE Trans. Circuits Syst. I*, vol. 45, pp. 574–577, May 1998.

[10] T. Hinamoto, "2-D Lyapunov equation and filter design based on the Fornasini–Marchesini second model," *IEEE Trans. Circuits Syst. I*, vol. 40, pp. 102–110, Feb. 1993.

[11] ——, "Stability of 2-D discrete systems described by the Fornasini–Marchesini second model," *IEEE Trans. Circuits Syst. I*, vol. 44, pp. 254–257, Mar. 1997.

[12] W.-S. Lu, "On a Lyapunov approach to stability analysis of 2-D digital filters," *IEEE Trans. Circuits Syst. I*, vol. 41, pp. 665–669, Oct. 1994.

[13] V. Singh, "A new realizability condition for limit cycle free state-space digital filters employing saturation arithmetic," *IEEE Trans. Circuits Syst.*, vol. CAS-32, pp. 1070–1071, Oct. 1985.

[14] ——, "On the realization of two's complement overflow limit cycle free state-space digital filters," *Proc. IEEE*, vol. 74, pp. 1287–1288, Sept. 1986.

Current-Feedback Amplifiers versus Voltage Operational Amplifiers

G. Palumbo and S. Pennisi

***Abstract*—This paper compares the main performance parameters of the current feedback opamp (CFOA) with those of a conventional voltage opamp (VOA). To make the comparison effective, a folded cascode VOA is considered (which is characterized by similar features and topology) and the same power consumption was assumed for both amplifiers. The work confirms that the CFOA can provide higher bandwidth, albeit at the expense of reduced loop gain. Noise performance is also analyzed. Input-referred noise generators are determined and some peculiar CFOA features, having no equivalence in conventional opamps, have been highlighted. It is shown that the CFOA has slightly lower noise voltage, but a larger noise current. Simulations are given which are in very good agreement with expected results.**

***Index Terms*—Amplifier noise, current feedback opamp, feedback amplifiers, operational amplifiers.**

I. Introduction

Current feedback opamp (CFOA) is becoming increasingly popular and more widely available [1]–[8], since it offers some advantages over conventional voltage opamp (VOA) in terms of bandwidth and slew rate [9]–[15].

A CFOA is constituted by three fundamental stages: two voltage buffers and a transimpedance stage. More specifically, the first buffer, whose input and output correspond to the noninverting and the inverting inputs of the CFOA, implements the input stage. The transimpedance

Manuscript received November 22, 1999; revised August 24, 2000. This paper was recommended by Associate Editor R. Gharpurey.

The authors are with the Dipartimento Elettrico Elettronico e Sistemistico, Università di Catania, I-95125 Catania, Italy (e-mail: gpalumbo@dees.unict.it; spennisi@dees.unict.it).

Publisher Item Identifier S 1057-7122(01)03852-1.

stage is the second stage. It converts the current, which flows to the output node of the input buffer into a voltage across a high-impedance node, thus determining the (transresistance) gain of the CFOA. The other voltage buffer implements the output stage and has the only purpose of properly driving the output load.

The high slew rate performance derives from the use of a class AB topology for both the input and output stages. Although differential stages with class AB capability, reported in the literature [16]–[19], could be used in conventional opamps to provide a high slew-rate, this option is rather unusual and expensive.

Despite the differences in topology structure between CFOA and VOA [20], [21], the external circuitry and applications are very similar. Indeed, a CFOA provides high gain between input and output, a high-resistance noninverting input, and a low-resistance output. These are also the fundamental characteristics of a VOA.

In this paper, a comparison is made between bipolar CFOA and VOA in regard to static, frequency and noise performance. Already published comparisons between different amplifier architectures have hitherto only considered ideal amplifiers or at least one-pole models [13], [22], with important parameters such as noise never being treated.

The comparison proposed assumes that actual CFOA behavior is characterized by a dominant pole and a second pole, limiting the amplifier gain-bandwidth product. The comparison is with a VOA of comparable topology, thus providing similar features. Moreover the electrical open- and closed-loop parameters of the amplifiers are related to the bias operating conditions, assuming the same power consumption for both amplifiers.

II. CFOA Characteristics

Consider the CFOA scheme diagram in Fig. 1(a). Transistors Q1–Q4 and Q9–Q12 form the input and output voltage buffers, respectively. The transimpedance stage is realized with the two Wilson current mirrors Q5–Q6 and Q7–Q8.

A. Static Performance

The small-signal model of the CFOA is shown in Fig. 1(b), where R_t is the equivalent resistance at the gain node A. The output resistance of the input voltage buffer, $1/g_{mi}$, is the input resistance at inverting node, and the input resistance of the input buffer, r_{b1}, is the input resistance of the noninverting node. The output resistance of the output voltage buffer, $1/g_{mo}$, is the output resistance. Controlled generators α_1, α_2 and h model the transfer functions of the input and output voltage buffer, and the complementary current mirror, respectively, and are usually almost unitary in module.

By inspection of Fig. 1(a), we get

$$R_t \approx \frac{\beta_n}{2} r_{c6} \left\| \frac{\beta_p}{2} r_{c8} = \frac{\beta_n \beta_p V_{An} V_{Ap}}{\beta_n V_{An} + \beta_p V_{Ap}} \frac{1}{2I_{B1}} \right. \tag{1}$$

$$\frac{1}{g_{mi}} = \frac{1}{g_{m3} + g_{m4}} = \frac{V_t}{2I_{B1}} \tag{2}$$

$$\frac{1}{g_{mo}} \approx \frac{V_t}{2I_o} \tag{3}$$

where

voltage V_t	thermal voltage (KT/q);
β_n, β_p	current gain of n and p transistors, respectively;
V_{An}, V_{Ap}	Early voltages of n and p transistors, respectively;
I_o	quiescent current in the output branch.

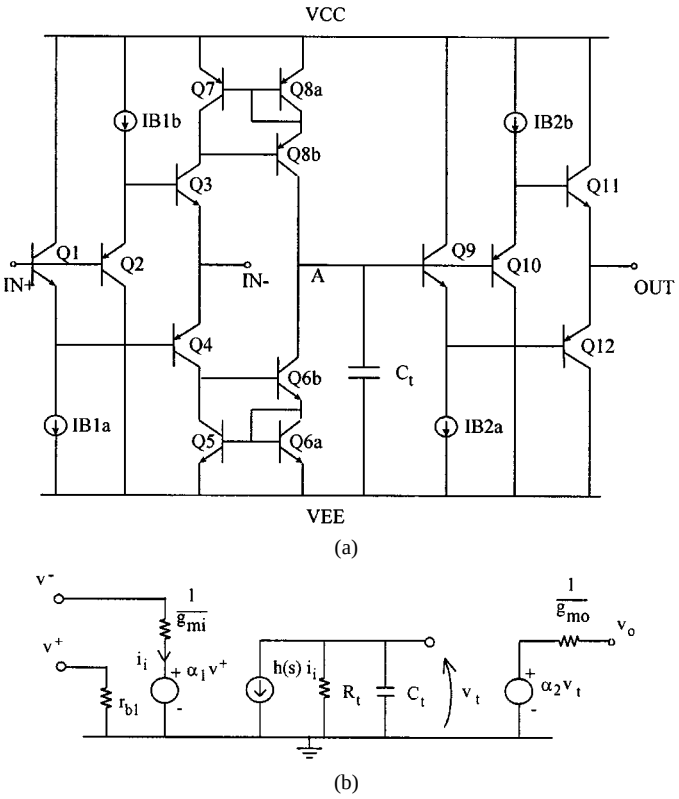

Fig. 1. (a) Scheme of the CFOA. (b) Small-signal model of the CFOA in Fig. 1(a).

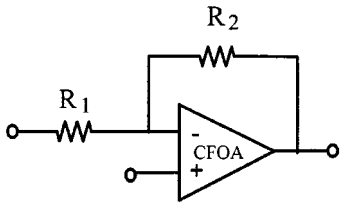

Fig. 2. Closed-loop configuration.

Providing a resistive feedback as shown in Fig. 2, the dc open-loop gain of the CFOA becomes

$$A_{olC} = \frac{R_1}{R_1 + \frac{1}{g_{mi}}} \frac{R_t}{R_2 + \frac{1}{g_{mo}} + \frac{1}{g_{mi}} \left\| R_1 \right.}$$

$$\approx \frac{R_t}{R_2 + \frac{1}{g_{mo}} + \frac{1}{g_{mi}}} \tag{4}$$

where the approximation holds if resistance R_1 is greater than $1/g_{mi}$. With this basic assumption the amplifier is always under unity gain current-feedback, irrespective of closed-loop gain (and R_1).

B. Frequency Performance and Stability

The dominant pole of the open-loop amplifier is

$$\omega_{dC} = \frac{1}{R_t C_t}. \tag{5}$$

From (4) and (5), the gain-bandwidth product results

$$\omega_{gbwC} \approx \frac{1}{\left(R_2 + \frac{1}{g_{mo}} + \frac{1}{g_{mi}}\right) C_t}. \tag{6}$$

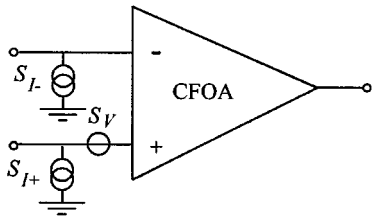

Fig. 3. Input noise generators of a CFOA.

Equation (6) shows the well-known property of CFOAs, The closed-loop bandwidth is independent of the closed-loop gain provided that resistance R_2 is maintained constant.

In order to guarantee stability providing a proper phase margin, φ, the relationship $\omega_{gbwC} = \omega_{2C}/\mathrm{tg}(\varphi)$ holds, where ω_{2C} is the equivalent second pole of the open-loop amplifier. Usually the second pole is at the output node due to load capacitance C_L

$$\omega_{2C} = \frac{1}{\left(R_2 + \frac{1}{g_{mi}} \middle\| R_1\right) \middle\| \frac{1}{g_{mo}} C_L}. \tag{7}$$

Hence, the worst case condition from a stability point of view, which is when the amplifier is operated in unity-gain loop (i.e., $R_2 = 0$, that makes the gain-bandwidth product the largest possible), sets [23]

$$C_t = \mathrm{tg}(\varphi)\, \frac{g_{mi}\, g_{mo}}{(g_{mi} + g_{mo})^2}\, C_L. \tag{8}$$

It is widely considered that a CFOA cannot be operated in unity-gain configuration using a resistance R_2 equal to zero. In our opinion this is not true. This misunderstanding derives from the fact that ideal CFOAs cannot be connected in such a fashion because two voltage generators (the output and the input buffer) would appear in parallel. However, real amplifiers include real buffers with finite (nonzero) output resistance. Therefore, the connection is not only possible, but also provides the highest open-loop gain and bandwidth (and minimum output noise). The issue now becomes to properly compensate the amplifier, and (8) gives the appropriate design equation.

Moreover, it is worth noting that for the same bandwidth (i.e., the same C_t) power consumption is minimized by setting $g_{mi} = g_{mo}$ which means $I_{B1} = I_{B2}$.

C. Noise Performance

Like conventional opamps, CFOA noise can be modeled by three equivalent input noise sources: a noise voltage generator and two noise current generators [20], [24], [25]. This model is shown in Fig. 3, where S_V, S_{I+} and S_{I-} are noise power spectral densities.

To evaluate the noise generators we use the transistor noise model with input-referred noise sources in Fig. 4. Neglecting flicker noise, parameters S_{Vj} and S_{Ij} in Fig. 4 are expressed respectively as

$$S_{Vj} = 4kT\left(r_{bj} + \frac{1}{2g_{mj}}\right) \tag{9a}$$

$$S_{Ij} \cong 2qI_{Bj} \tag{9b}$$

where r_{bj} and I_{Bj} are the base resistance and the quiescent base current of the jth transistor, respectively.

Observe that the evaluation of input noise generators is complicated by the fact that a CCII is a three-terminal device where terminal X acts as an input (current) and output (voltage) terminal at the same time.

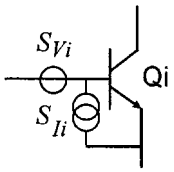

Fig. 4. Bipolar transistor with equivalent noise generators.

Therefore, care must be taken when evaluating the equivalent output voltage noise at terminal X, to separate the component due to noise voltage from that due to noise current.

CFOA input noise voltage, S_V, can be computed by evaluating the open-circuit voltage at the inverting terminal with the noninverting one grounded. It is equal to the input noise of the voltage follower Q1–Q4. Calculation is simplified by considering that all the input transistors have the same quiescent collector current. They are thus characterized by the same transconductance $g_m = g_{mi}$.

$$\begin{aligned} S_V &\approx \left(\tfrac{1}{2}\right)^2 \\ &\quad \cdot \left[2S_{V1,3} + 2S_{V2,4} + \frac{1}{g_{mi}^2} \right. \\ &\quad \left. \cdot \left(S_{IB1a} + S_{IB1b} + S_{I1} + S_{I2} + \frac{1}{4}S_{I3} + \frac{1}{4}S_{I4}\right)\right] \\ &\approx 4kT\left(r_b + \frac{V_T}{2I_C}\right). \end{aligned} \tag{10a}$$

Let us now consider the two noise current generators S_{I+} and S_{I-}. As known, these equivalent sources are exactly equal for conventional opamps. For CFOAs, however, the asymmetry of the input stage leads to two very different values. The current generator at the noninverting (high-impedance) input can be found by evaluating the short-circuit current at the same input terminal (as for conventional VOAs). In contrast, the equivalent noise generator at the inverting input (which can be seen as the input referred noise of the current follower between terminal in- and node A) can be found by evaluating the short-circuit current at node A (with the input terminals left open). We get

$$\begin{aligned} S_{I-} &\approx 2g_{mi}^2\left(S_{V5,6} + S_{V7,8}\right) + S_{I9} + S_{I10} \\ &\quad + \frac{1}{\beta_{NPN}^2} S_{IB2a} + \frac{1}{\beta_{PNP}^2} S_{IB2b} \\ &\approx 16kTg_{mi}^2\left(r_b + \frac{1}{2g_{mi}}\right) \\ &= 16\left(r_b\frac{I_C}{V_T} + \frac{1}{2}\right)qI_C \end{aligned} \tag{10b}$$

$$\begin{aligned} S_{I+} &\approx S_{I1} + S_{I2} + \frac{1}{\beta_{NPN}^2} S_{IB1a} + \frac{1}{\beta_{PNP}^2} S_{IB1b} \\ &\approx 2\left(\frac{1}{\beta_{NPN}} + \frac{1}{\beta_{PNP}}\right)qI_C \end{aligned} \tag{10c}$$

where S_{IBj} represents the parallel noise of the jth bias current generator.

Equations (10a)–(10c) indicate weakly correlated noise expressions. As known, this is a favorable condition which greatly simplifies noise computation and makes the definition of input noise generators quite useful. Moreover, by comparing (10b) and (10c) it can be easily recognized that the noise current of the inverting input is much higher than that of the noninverting one.

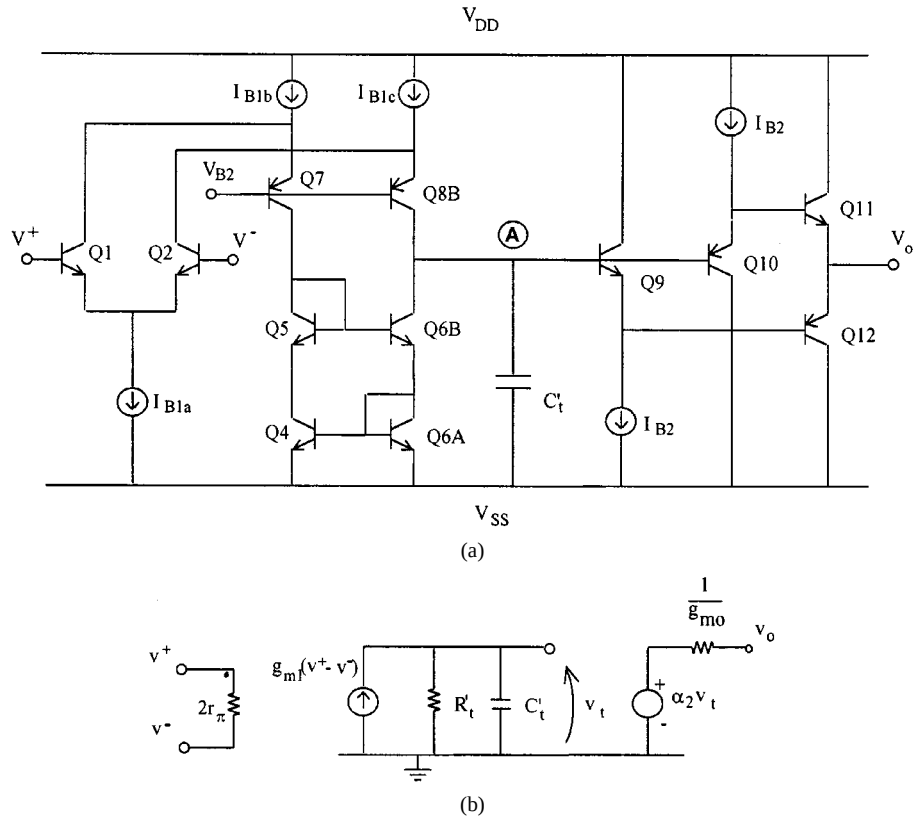

Fig. 5. (a) Scheme of the VOA. (b) Small-signal model of the VOA.

We now evaluate the total output noise in a generic closed loop configuration with resistive feedback, by using the noise model developed. In a closed-loop configuration, assuming an infinite open-loop gain, the noise is transferred to the output exclusively via the feedback network. Therefore, for the circuit in Fig. 2 the output noise power spectral density is

$$S_o = \left(1 + \frac{R_2}{R_1}\right)^2 S_V + S_{I-} R_2^2 + S_{VR1} \left(\frac{R_2}{R_1}\right)^2 + S_{VR2} \quad (11)$$

where S_{VRj} is the thermal noise voltage of the jth resistor, $4kTR_j$. Equation (11) is the same well-known expression of the output noise power spectral density as for the VOA and well approximates the output noise for R_2 much greater than $1/g_{mi}$.

III. VOA Characteristics

In order to compare the CFOA with a VOA, we consider a VOA architecture with features similar to those of the CFOA analyzed previously. In particular, the topology chosen is the *folded cascode* VOA in Fig. 5(a). The main characteristic of this topology is, like the CFOA in Fig. 1(a), having only one high-gain stage, since it achieves the high voltage gain thanks to the high equivalent resistance at node A. Moreover, the fully transconductance of the input differential stage is gained by using the Wilson current mirror Q4–Q6, to perform a differential-to-single conversion.

A. Static Performance

The equivalent small-signal model of the VOA considered is shown in Fig. 5(b), where R_t' and C_t' are the equivalent resistance and the compensation capacitance at the gain node, respectively, and $2r_\pi$ is the equivalent resistance at the input of the differential stage Q1–Q2. The transconductance gain, g_{m1}, is equal to that of the input transistors Q1, Q2, with the other parameters being defined previously.

Model parameters are related to the bias operating point through the following relationships

$$R_t' \approx \frac{\beta_n}{2} r_{c6} \Big\| \beta_p r_{c8} = \frac{\beta_n \beta_p V_{An} V_{Ap}}{\beta_n V_{An} + 2\beta_p V_{Ap}} \frac{1}{I_{B1}} \quad (12)$$

$$r_\pi = \frac{V_t}{\beta_n I_{Ba1}} \quad (13)$$

$$g_{m1} = \frac{I_{B1a}}{V_t} \quad (14)$$

and applying a resistive feedback as shown in Fig. 2, the dc open-loop gain is

$$A_{olV} = \frac{2r_\pi \| R_1}{R_2 + \dfrac{1}{g_{mo}} + 2r_\pi \Big\| R_1} g_{m1} R_t' \approx \frac{g_{m1} R_t'}{G_\infty} \quad (15)$$

where G_∞ represents the asymptotic gain

$$G_\infty = 1 + \frac{R_2}{R_1}. \quad (16)$$

B. Frequency Performance and Stability

The dominant pole of the open-loop amplifier is again given by (5) substituting R_t' and C_t' for R_t and C_t. Thus, the gain-bandwidth product results

$$\omega_{gbwV} \approx \frac{g_{m1}}{G_\infty C_t'}. \quad (17)$$

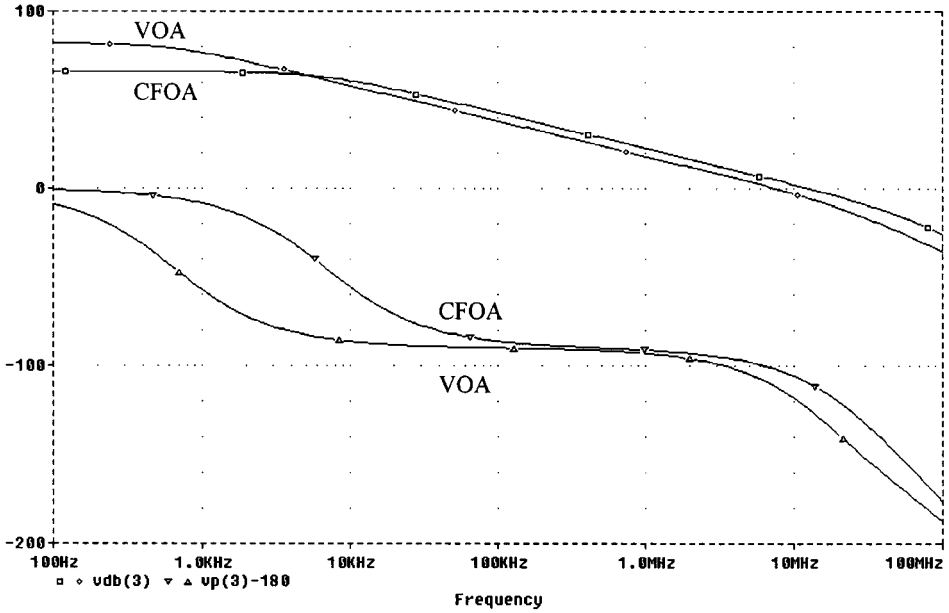

Fig. 6. Frequency responses of the loop-gain of CFOA and VOA.

For VOA, too, the second pole of the loop-gain can be assumed at the output and is given by

$$\omega_{2C} = \frac{1}{(R_2 + R_1)\left\| \frac{1}{g_{mo}} C_L \right.} \approx \frac{g_{mo}}{C_L}. \tag{18}$$

Hence, to achieve the phase margin φ in the worst condition of unity-gain loop, the compensation capacitance

$$C_t' = \mathrm{tg}(\varphi)\, \frac{g_{m1}}{g_{mo}}\, C_L \tag{19}$$

is needed.

C. Noise Performance

Conventional VOAs are by nature low noise configurations. Indeed, the input stage provides maximum power gain, which reduces the noise contribution of the following stages. Therefore, the input referred noise is practically only due to the input stage. In particular, we get

$$S_V \approx 2S_{V1,2} + 2\, \frac{g_{m4,6}^2}{g_{m1}^2}\, S_{V4,6} + \frac{S_{IB1b} + S_{IB1c}}{g_{m1}^2} \tag{20a}$$

$$S_{I+} = S_{I-} = S_{I1,2}. \tag{20b}$$

Equivalent noise voltage in (20a) can be simplified by using low-noise bias current generators and setting $g_{m4,6} \gg g_{m1}$. However, in our design $g_{m4,6} = g_{m1}$ is chosen, thus giving a VOA voltage power noise which is twice that of the CFOA.

For purely resistive closed-loop configurations, the total output noise is still given by (11) which was already derived for the CFOAs.

IV. Comparison

Since a tradeoff exists between frequency performance and power dissipation (and sometimes between gain and power dissipation), we assume, without loss of generality, the same power consumption for both the CFOA and VOA by setting $I_{B1a,b,c}$ equal to $2I_{B1}$. As a consequence, the VOA input transconductance results

TABLE I
Equivalent Input Noise Generators of CFOA and VOA

Noise	CFOA		VOA	
	Simul.	Calcul.	Simul.	Calcul.
$\sqrt{S_V}$ (nV/$\sqrt{\text{Hz}}$)	2.1	2.8	6.0	5.5
$\sqrt{S_{I-}}$ (pA/$\sqrt{\text{Hz}}$)	40	43	0.8	0.8
$\sqrt{S_{I+}}$ (pA/$\sqrt{\text{Hz}}$)	1.7	1.7	0.8	0.8

$$g_{m1} = g_{mi} = g_{mo} = g_m. \tag{21}$$

Thus, the VOA resistance R_t' is in the range $R_t < R_t' < 2R_t$ (it is equal to $2R_t$ if a cascode current mirror is used in the VOA instead of a Wilson current mirror).

The dc value of the open-loop gain directly sets the accuracy of the closed-loop transfer functions. For instance, when the amplifiers are operated in unity-gain configuration, the open-loop gain determines the transfer error $A_{ol}/(1 + A_{ol})$.

Comparing the open-loop gain of the CFOA with that of the VOA, we get

$$\frac{A_{olC}}{A_{olV}} = \frac{R_t}{R_t'}\, \frac{G_\infty}{2 + g_m R_2} \tag{22}$$

which is *always* much lower than one, as $g_m R_2 >> R_2/R_1$. This means that for the same amount of power consumption the (closed-loop) accuracy of a bipolar CFOA is worse than that achieved with a VOA. The ratio given by (22) is equal to its maximum, i.e., $R_t/2R_t'$, for the amplifiers used in unity-gain configuration.

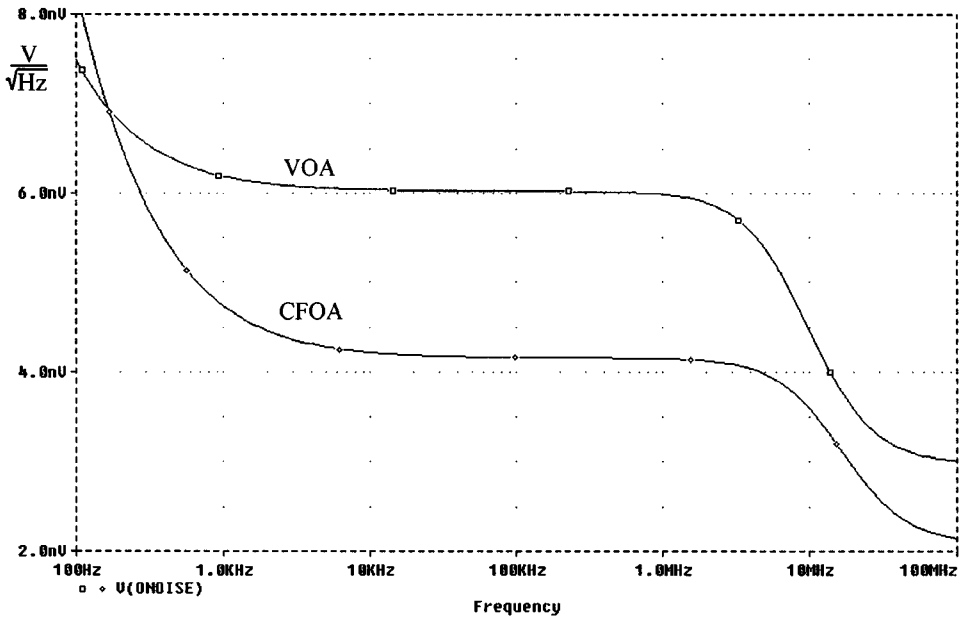

Fig. 7. Output noise of the CFOA and VOA, in unity-gain configuration ($R_2 = 0$).

By comparing the resulting bandwidth of the CFOA and VOA we get

$$\frac{\omega_{dC}}{\omega_{dV}} = \frac{R_t' C_t'}{R_t C_t} = 4\,\frac{R_t'}{R_t} \tag{23}$$

which shows the CFOA bandwidth is superior to that of the VOA, for the same power consumption. This advantage in terms of speed is achieved in an open-loop configuration, but to really evaluate the speed benefit we have to compare the CFOA and VOA frequency response in a closed-loop configuration. The closed-loop bandwidth is equal to the gain-bandwidth product of the open-loop gain, and, hence, we can simply compare the gain-bandwidth product of the two amplifiers. Thus, we get

$$\frac{\omega_{gbwC}}{\omega_{gbwV}} = 4\,\frac{G_\infty}{2 + g_m R_2}. \tag{24}$$

Equation (24) reveals that when the amplifiers are used in unity-gain configuration (with R_2 equal to zero), the CFOA gain-bandwidth product is only twice as great as that of the VOA considered. The bandwidth improvement can be higher for closed-loop gains greater than 1. In this case, remembering the definition of G_∞ the expression in (24) can be rewritten as

$$\frac{\omega_{gbwC}}{\omega_{gbwV}} = 4\,\frac{G_\infty}{2 + g_m R_1 (G_\infty - 1)}. \tag{25}$$

Assuming as usual $gmR1 \gg 1$, (25) shows a gain-bandwidth ratio lower than 4 in any case.

As far as the noise performance is concerned, by comparing (10a)–(10c) and (20) it becomes apparent that similar noise voltage and noise currents at the noninverting input characterize the two circuits. We have already outlined a first difference between the CFOA and VOA due to the nonsymmetrical CFOA input stage leading to two different input equivalent noise currents. The noise current given in (10b) is considerably higher than the one in (20b), since it represents the noise of a class AB current mirror. Due to the higher relative value of S_{I-} the closed-loop output noise of CFOA can rise dramatically, especially for high values of the feedback resistance R_2. In particular, it can be shown that the contribution to the output noise of S_{I-} becomes greater than that of S_V if resistance R_2 is greater than $G_\infty/2g_m$. As one may easily realize, this condition is usually met and then the output noise in CFOA is dominated by the noise current.

Another difference concerns the noise of the bias current generators. Equations (10a) and (10c) state that the noise current from IB1 and IB2 affects the CFOAs equivalent input noise. For VOAs, however, the same component is partially suppressed by the CMRR. In fact, the noise current of IB1a does not appear in the equivalent input noise expressions. In addition, (10b) shows that the equivalent noise input current of the output stage also adds directly to S_{I-}. This aspect is completely absent in VOAs, where the noise is due to the input stage only, but it was already encountered in other current-mode amplifiers [24]. This noise component can become significant if high bias currents are used in the output stage, but can be decreased using mirrors (Q5–Q6 and Q7–Q8) whose current ratios are greater than one [25].

V. Simulation Results

To validate the above discussion, the two opamps in Figs. 1(a) and 5(a) were implemented using standard bipolar technology with maximum current gain and transition frequency of npn transistors equal to 90 and 4 GHz, and those of pnp transistors equal to 30 and 2.4 GHz. The base resistance was about 400 Ω for both transistors. We used a power supply of 5 V and the bias currents IB1 and IB2 were set equal to 200 μA. To have the same VOA power dissipation (of about 7 mW), the bias current of the differential pair, IB1a, was set to 400 μA. With the above bias conditions the output resistances (as well as the inverting input resistance for the CFOA), resulted 80 Ω. Assuming a load capacitor of 100 pF, and imposing a phase margin of 70°, the compensation capacitors required, as given by (8) and (19) for the CFOA and VOA, were 69 pF and 138 pF, respectively.

Fig. 6 illustrates the loop gain of the two amplifiers assuming unity gain configuration. The dc gain is 66 dB and 82 dB, a strong degradation of gain is manifest in the CFOA, just as predicted by (22). The gain-bandwidth of the CFOA is about 14 MHz, while it is only 7 MHz for the VOA. As expected from (24) the gain-bandwidth of the CFOA is greater by a factor about equal to 2. Finally, a very good agreement

TABLE II
OUTPUT NOISE OF VOA AND CFOA FOR DIFFERENT CLOSED-LOOP GAINS AND FEEDBACK RESISTANCES

$\sqrt{S_{Vo}}$ (nV/$\sqrt{\text{Hz}}$) (only white noise)			
R_1 (kΩ)	R_2 (kΩ)	CFOA	VOA
0.5	5	206	73
	10	373	136.6
	15	493.1	194.6
1	10	546	80
	20	550	150
	30	649.7	213.7

between the simulated and expected phase margins was found. Error was only about 0.1° for both the CFOA and VOA.

Slew rate was found to be one order of magnitude higher for the CFOA (equal to 29 V/μs), whereas that of the VOA (equal to 3 V/μs) is limited by the bias current of the class A input stage.

Table I reports the spectral densities of input noise voltage and current generators for both amplifiers. As can be seen, the simulated values are in good agreement with the ones calculated using (10a)–(10c) and (20). The VOA noise voltage is about twice that of the CFOA, the noise currents of VOA are also twice those associated to the noninverting input of the CFOA, while the noise current at the inverting CFOA input is about 50 times greater than that of its VOA counterpart.

Fig. 7 shows the output noise voltage spectral density for both amplifiers in unity-gain closed-loop configuration. The white noise contribution is 4.2 nV/$\sqrt{\text{Hz}}$ and 6 nV/$\sqrt{\text{Hz}}$ for the CFOA and VOA, respectively. For unity gain, the CFOA has better noise performance due to its lower input equivalent noise voltage. However, as already noted, the higher CFOA noise current S_{I-} can be responsible of significant output noise, for increasing values of resistance R_2. This is confirmed by the data given in Table II, which reports the output (white) noise of the CFOA and VOA, for different closed-loop gains and feedback resistances.

VI. CONCLUSIONS

A detailed comparison between a CFOA and a VOA with comparable topology, was presented in this paper. Electrical open- and closed-loop parameters were related to bias operating conditions, assuming the same power consumption for both amplifiers. The work confirms that the CFOA provides a higher gain-bandwidth product. However, this was achieved at the expense of losing open-loop gain. Specifically, it was found that the ratio between the CFOA and VOA dc open-loop gain decreases on increasing feedback resistance R_2. For R_2 equal to zero the ratio reaches its maximum which is equal to $R_t/2R_t'$, of which R_t and R_t' are the small-signal resistances at the high impedance internal node of the CFOA and VOA, respectively. In this case, the gain-bandwidth product of the CFOA is twice as large as the VOA (and in general, never higher than four times).

A comparison of the noise characteristics was also carried out and some peculiar CFOA features, with no equivalence in conventional opamps, were highlighted. The CFOA employs a common-base configuration to implement a current-in stage which has no current gain. Therefore, a considerably worse noise current was found for this amplifier, while noise voltage was similar to that of the VOA. For R_2 greater than $G_\infty/2g_m$ (a usually met condition), the output closed-loop noise of the CFOA is dominated by the noise current contribution.

All the analytical results which were developed in this work were lastly validated through simulations using SPICE. A very good agreement between the expected data and simulations was encountered.

ACKNOWLEDGMENT

The authors wish to thank the anonymous reviewers for their useful comments, which contributed to significantly improve the quality of the original manuscript.

REFERENCES

[1] J. Haslett, M. Rao, and L. Bruton, "High-frequency active filter design using monolithic nullors," *IEEE J. Solid-State Circuits*, vol. SC-15, pp. 955–962, Dec. 1980.
[2] C. Tomazou, F. Lidgey, and D. Haigh, Eds., *Analogue IC Design: The Current-Mode Approach*. London, U.K.: IEE, 1990.
[3] A. Fabre, "Gyrator implementation from commercially available transimpedance operational amplifiers," *Electron. Lett.*, vol. 28, no. 3, pp. 263–264, 1992.
[4] ——, "Insensitive voltage-mode and current-mode filters from commercially available transimpedance opamps," *Proc. Inst. Electr. Eng. G.*, vol. 140, no. 5, pp. 116–130, 1993.
[5] S. Celma, P. Martinez, and A. Carlosena, "Current feedback amplifiers based sinusoidal oscillator," *IEEE Trans. Circuits Syst. I*, vol. 41, pp. 906–908, Dec. 1994.
[6] M. Abuelma'atti, A. Farooqi, and S. Alshahrani, "Novel RC oscillators using the current-feedback operational amplifier," *IEEE Trans. Circuits Syst. I*, vol. 43, pp. 155–157, Feb. 1996.
[7] R. Senani and V. Singh, "Novel single-resistance-controlled-oscillator configuration using current feedback amplifiers," *IEEE Trans. Circuits Syst. I*, vol. 43, pp. 698–700, Aug. 1996.
[8] A. Soliman, "Applications of the current feedback operational amplifiers," *Analog Integr.Circuits Signal Process.*, vol. 16, no. 11, pp. 265–302, 1996.
[9] S. Soclof, *Design and Applications of Analog Integrated Circuits*. Englewood Cliffs, NJ: Prentice-Hall, 1991.
[10] D. Smith, M. Koen, and A. Witulski, "Evolution of high-speed operational amplifier architectures," *IEEE J. Solid-State Circuits*, vol. 29, pp. 1166–1179, Oct. 1994.
[11] C. Toumazou and J. Lidge, "Current feedback op-amps: A blessing in disguise?," *IEEE Circuits Devices Mag.*, pp. 34–37, Jan. 1994.
[12] B. Wilson, "Constant bandwidth voltage amplification using current conveyor," *Int. J. Electron.*, vol. 65, no. 5, pp. 983–988, 1988.
[13] E. Bruun, "Feedback analysis of transimpedance operational amplifier circuits," *IEEE Trans. Circuits Syst. I*, vol. 40, pp. 275–277, Apr. 1993.
[14] S. Franco, "Analytical foundation of current-feedback amplifiers," in *Proc IEEE ISCAS'93*, San Francisco, CA, 1993, pp. 1050–1053.
[15] A. Arbel, "Negative feedback revisited," *Analog Integr.Circuits Signal Process.*, vol. 16, no. 10, pp. 157–178, 1996.
[16] E. Seevinck and R. F. Wassenaar, "A versatile CMOS linear transconductor/square-law function circuit," *IEEE J. Solid-State Circuits*, vol. SC-22, pp. 366–377, June 1987.
[17] K. Bremer and J. Wieser, "Large swing CMOS power amplifier," *IEEE J. Solid-State Circuits*, vol. SC-18, pp. 624–629, Dec. 1983.
[18] R. Castello, "CMOS buffer amplifier," *Analog Circuit Design*, pp. 113–138, 1993.
[19] G. Caiulo, F. Maloberti, G. Palmisano, and S. Portaluri, "Video CMOS power buffer with extended linearity," *IEEE J. Solid-State Circuits*, vol. 28, pp. 845–848, July 1993.
[20] P. Gray and R. Meyer, *Analysis and Design of Analog Integrated Circuits*, 3rd ed. New York: Wiley, 1993.
[21] K. Laker and W. Sansen, *Design of Analog Integrated Circuits and Systems*. New York: McGraw-Hill, 1994.
[22] A. Payne and C. Toumazou, "Analog amplifiers: Classification and generalization," *IEEE Trans. Circuits Syst. I*, vol. 43, pp. 43–50, Jan. 1996.
[23] G. Palumbo, "Bipolar current feedback amplifier: Compensation guidelines," *Analog Integr.Circuits Signal Process.*, vol. 19, no. 2, pp. 107–114, 1999.
[24] A. Arbel, "Comparison between the noise performance of current-mode and voltage-mode amplifiers," *Int. J. Analog Integr.Circuits Signal Process.*, vol. 7, no. 7, pp. 221–242, 1995.
[25] E. Bruun, "Analysis of the noise characteristics of CMOS current conveyors," *Analog Integr.Circuits Signal Process.*, vol. 17, no. 12, pp. 71–78, 1997.